Bi-Scale Appearance Fabrication

Yanxiang Lan* Yue Dong† Fabio Pellacini‡§ Xin Tong†

*Tsinghua University †Microsoft Research Asia ‡Dartmouth College §Sapienza University of Rome
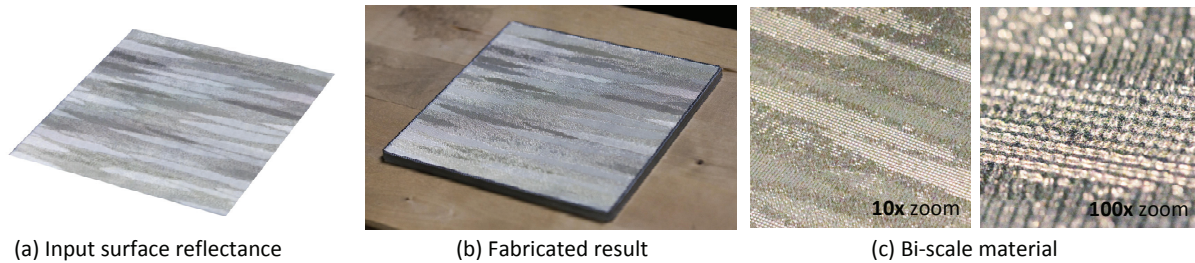
(a) Input surface reflectance   (b) Fabricated result   (c) Bi-scale material

Figure 1: *Given an input surface reflectance (a) with anisotropic BRDFs and per-point shading frame variations, our system prints a bi-scale material (b) to reproduce the input surface reflectance. The bi-scale material consists of a small scale height field covered with isotropic BRDFs as shown in (c).*

Abstract

Surfaces in the real world exhibit complex appearance due to spatial variations in both their reflectance and local shading frames (i.e. the local coordinate system defined by the normal and tangent direction). For opaque surfaces, existing fabrication solutions can reproduce well only the spatial variations of isotropic reflectance. In this paper, we present a system for fabricating surfaces with desired spatially-varying reflectance, including anisotropic ones, and local shading frames. We approximate each input reflectance, rotated by its local frame, as a small patch of oriented facets coated with isotropic glossy inks. By assigning different ink combinations to facets with different orientations, this bi-scale material can reproduce a wider variety of reflectance than the printer gamut, including anisotropic materials. By orienting the facets appropriately, we control the local shading frame. We propose an algorithm to automatically determine the optimal facets orientations and ink combinations that best approximate a given input appearance, while obeying manufacturing constraints on both geometry and ink gamut. We fabricate the resulting surface with commercially available hardware, a 3D printer to fabricate the facets and a flatbed UV printer to coat them with inks. We validate our method by fabricating a variety of isotropic and anisotropic materials with rich variations in normals and tangents.

CR Categories: I.3.7 [Computer Graphics]: Three-Dimensional Graphics and Realism—Color, shading, shadowing, and texture;

Keywords: fabrication, bi-scale, SVBRDF, local frame, normal map

Links: ◆DL 🗋PDF

1 Introduction

Fabricating Surface Appearance. Real-world surfaces have rich and detailed appearance that comes from the interaction of geometric details and spatially-varying reflectance. Most research efforts have focused on how to capture, model and render complex appearance to improve synthetic imagery [Dorsey et al. 2008]. Recent advances in computer-controlled rapid prototyping hardware, today capable of printing complex shapes, are motivating investigations on how to physically reproduce the appearance of object surfaces, either scanned or designed. In this paper we focus on opaque surfaces that exhibit spatially-varying changes to both the local shading frames, namely normals and tangents, and to the reflectance, described in this case by the bidirectional reflectance distribution function (BRDF).

Several methods have been proposed for fabricating custom surface reflectance. Weyrich et al. [2009] reproduce the micro-scale geometry of a BRDF with a tilable continuous height field and manufacture the result using a milling machine. Matusik et al. [2009] present a solution for printing isotropic spatially-varying reflectance over a flat surface by mixing isotropic inks. Although in principle these solutions can be extended to print a wide range of BRDFs, the high resolution geometry or large ink set needed for modeling each BRDF makes these solutions infeasible for printing geometric surface details and anisotropic reflectance variations in practice.

Bi-Scale Appearance Fabrication. In this paper, we present a method for fabricating a surface with spatially-varying opaque reflectance and shading frames, described by a spatially-varying BRDF (SVBRDF) with per-point normal and tangent directions. Our method is based on the key observation that each single BRDF can be efficiently modeled as the average appearance of a compact small-scale patch composed of oriented facets, each covered with a homogeneous BRDF chosen from a fixed set. By assigning different BRDFs to facets with different orientations, this bi-scale material is capable of reproducing a much wider variety of surface reflectance than is captured by the printer gamut alone, including anisotropic BRDFs. By orienting the facets appropriately, we can also control the local shading frame at that surface location. We reproduce the input surface reflectance with spatially-varying bi-scale material fabricated as a small-scale axis-aligned height field whose facets are covered by the isotropic BRDFs of glossy printer inks. Given the manufacturing constraints, namely the maximum

height field resolution and the BRDF gamut of the printer ink set, we present an algorithm to compute the height field and facet ink combinations of the bi-scale material that best approximate the input appearance, both in terms of reflectance and shading frames. We fabricate the height field with a 3D printer and subsequently print the glossy BRDFs over each facet with a flatbed UV printer. Figure 1 shows a surface with anisotropic SVBRDFs manufactured with our system.

We compute the optimal height field and ink combinations by solving an optimization problem that minimizes the difference between the input reflectance and the reflectance of the fabricated bi-scale material. The optimization is non-linear since the reflectance of the bi-scale material is non-linearly related to the parameters we want to estimate. Solving this optimization presents two main challenges. First, the optimization has a strong non-linear nature and we need to estimate a large number of parameters, namely all possible combinations of facet orientations and BRDFs. Second, due to the shadowing and masking effects of the height field, the reflectance of the bi-scale material of one patch also depends on the neighboring patches. Thus the parameters of all patches need to be optimized together. We solve this optimization problem in three steps, each of which provides a good initialization for the one following. We first treat the BRDFs and shading frames independently and fit the input BRDFs, aligned to a global frame, and then compute the optimal height field and ink BRDFs for the patch at each location. We then rotate each bi-scale patch back to its shading frame and iteratively optimize both height field and ink combinations in the rotated frame. After these two steps, we obtain the optimal bi-scale patch for each individual pixel. We finally tile all samples together and perform a global optimization to account for inter-patch effects and to generate a continuous height field.

We validate our solution by printing surfaces with both captured and designed appearance. Our results show that our method can reproduce well detailed surface appearance from spatially-varying reflectance, both isotropic and anisotropic, and local shading frame variations. The main contributions of our work are (a) a bi-scale material representation for reproducing surface appearance with anisotropic and shading frame variations, (b) an optimization method for computing the height field and ink combinations from the input surface reflectance and (c) a hardware solution for printing the bi-scale material.

2   Related Work

Appearance Fabrication   Various methods have been developed for fabricating materials with custom surface reflectance [Weyrich et al. 2009; Matusik et al. 2009], subsurface scattering [Hašan et al. 2010; Dong et al. 2010], and reflectance functions [Malzbender et al. 2012].

Weyrich et al. [2009] model the micro-structure of a BRDF directly with a continuous height field and fabricate the surface via a milling machine. Since a high resolution height field is always required for simulating the appearance of a single BRDF, this method is impractical for fabricating spatially-varying surface reflectance. Also the shadowing and masking effects of the height field are ignored and this decreases the fidelity of the printed object. Matusik et al. [2009] approximate the target SVBRDFs by combining inks with known BRDFs. Although this works well for isotropic BRDFs, it cannot reproduce the appearance of anisotropic BRDFs or BRDFs with different normal or tangent directions. Hullin et al. [2011] present a method for displaying dynamic BRDFs with liquid surfaces, which is impractical to combine with other 3D printing technologies. These methods reproduce SVBRDFs at a single scale. Our approach differs from them in that we model the surface re-

flectance with a bi-scale solution by combining the appearance of a small scale height field and its isotropic BRDFs. Our method trades off spatial resolution to model reflectance with different angular variations. Furthermore, our method takes the shadowing and masking effects of the height field into consideration and thus can better predict the resulting appearance.

Recently, Malzbender et al. [2012] presented a method for printing the 4D reflectance function of a surface for a fixed viewing direction. For each input pixel, its appearance variation under different lighting directions is reproduced by coated reflective dimples. Although this method can reproduce arbitrary appearance variations under different lighting directions, it cannot be extended to the case of 6D SVBRDFs.

Fabrication for Image Display   Other methods fabricate geometric shapes and materials for displaying custom image contents. Alexa and Matusik [2010] construct diffuse relief surfaces for displaying one or two given images under different directional lighting. Bermano et al. [2012] exploit the self-shadowing of a relief surface lit from certain directions to display several prescribed images. Papas et al. [2012] constructed refractive lens arrays to reveal hidden images from an unstructured image underneath the lens. These methods can only display a discrete set of images and cannot be extended to exhibit continuous appearance variations under different lighting and viewing directions. Holroyd et al. [2011] converted a 3D model into a fabricated multilayer model that can display the 3D shape of an object under a wide range of viewing directions. Regg et al. [2010] fabricated the surface with designed grooves so that its highlights under a given lighting direction display 3D shape and motion parallax under different viewing directions. In these methods, the appearance of the displayed object surface is diffuse. Recently, Dong et al. [2012] printed custom SVBRDFs for displaying the appearance of HDR images at different exposures. To print custom surface reflectance, their method shares the same limitations of [Matusik et al. 2009].

Physically-based Material Modeling   Early methods [Westin et al. 1992; Gondek et al. 1994] directly compute surface reflectance from given small scale geometric structures via offline rendering. Ashkhmin [2000] developed a method to model the BRDF from a given microfacet distribution. Heidrich et al. [2000] simulated the BRDF of a height field with precomputed visibility. Wu et al. [2009] presented a scheme to quickly render the average appearance of small scale geometry and its BRDFs. Later they presented a technique for interactively editing the geometry and BRDF of a physically based bi-scale material [Wu et al. 2011]. They also realized their designs with diffuse BRDFs and manually folded geometry. Zhao et al. [2011] modeled cloth appearance with small scale geometry captured by micro CT imaging and then designed the new cloth appearance by geometry structure synthesis [Zhao et al. 2012]. Most recently, Iwasaki et al. [2012] presented a technique for rendering and editing bi-scale materials under all frequency lighting in real time. All these methods assume the geometry and BRDFs are known.

Our method is inspired by these physically based material modeling works but targets a different goal. Instead of computing the averaged surface reflectance from a known geometric structure with material properties manually designed by users, our method automatically derives a geometry structure and its material properties from an averaged surface reflectance.
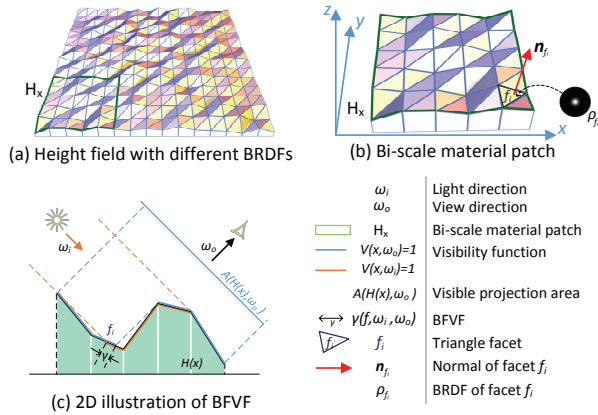
ω_i	Light direction
ω_o	View direction
$H_{\mathbf{x}}$	Bi-scale material patch
$V(x,\omega_o)=1$	Visibility function
$V(x,\omega_i)=1$	
$A(H(x),\omega_o)$	Visible projection area
$\gamma(f,\omega_i,\omega_o)$	BFVF
f_i	Triangle facet
$\mathbf{n}_{f_i}$	Normal of facet f_i
ρ_{f_i}	BRDF of facet f_i

Figure 2: *Bi-scale material. (a) Our bi-scale material is represented by a small scale axis-aligned height field whose facets are covered by a homogeneous BRDF of glossy printer inks. (b) A small square patch $H_{\mathbf{x}}$ of bi-scale material for modeling input surface reflectance at a single point. (c) 2D illustration of the BFVF of facets and the terms used in computing the effective BRDF of a bi-scale material.*

3 Bi-scale Representation

Input Surface Reflectance The input to our system is a spatially-varying BRDF $\rho_i(\mathbf{x}, \omega_i', \omega_o')$ and the local shading frames determined by the normal $\mathbf{n}_{\mathbf{x}}$ and tangent $\mathbf{t}_{\mathbf{x}}$ at each location $\mathbf{x}$ (we use primed angles to indicate values in the local frames). We denote the BRDF rotated by the local frame as $\rho(\mathbf{n}_{\mathbf{x}}, \mathbf{t}_{\mathbf{x}}, \mathbf{x}, \omega_i, \omega_o)$. In this notation, incoming and outgoing angles are defined in the global frame and are rotated by the local frame before evaluating the BRDF ρ_i. Given the input surface appearance, the reflected radiance L at $\mathbf{x}$ along a view direction ω_o can be computed by

$$L(\mathbf{x}, \omega_o) = \int_{\Omega_{\mathbf{x}}} \rho(\mathbf{n}_{\mathbf{x}}, \mathbf{t}_{\mathbf{x}}, \mathbf{x}, \omega_i, \omega_o) L_i(\mathbf{x}, \omega_i)(\mathbf{n}_{\mathbf{x}} \cdot \omega_i) \mathrm{d}\omega_i, \quad (1)$$

where $\Omega_{\mathbf{x}}$ is the upper hemisphere, L_i is the incident radiance, and $(\cdot)$ is the dot product of two vectors clamped to zero if negative. We assume that the input surface reflectance is sampled on an $N_x \times N_y$ regular grid on the XY plane.

Output Bi-scale Material We reproduce the appearance of the input reflectance by manufacturing a surface $H = (h, \rho_h)$ as a height field h coated by a spatially-varying BRDF ρ_h. The appearance of the fabricated surface, shown in Figure 2.a, comes from the bi-scale interaction between the facet orientations and the ink BRDFs. We represent the height field as an axis aligned triangle mesh. For each triangle, the whole facet is coated with the same ink combination and thus has the same BRDF, while different triangles can be printed with different ink combinations. In our system, the input surface reflectance ρ at each point $\mathbf{x}$ is approximated by the effective BRDF $\bar{\rho}$ of a small square patch $H_{\mathbf{x}}$ of bi-scale material H. The effective BRDF $\bar{\rho}$ is the spatial average of the surface reflectance of the facets in $H_{\mathbf{x}}$ that are visible along both ω_i and ω_o (Figure 2.b):

$$\bar{\rho}(H_{\mathbf{x}}, \omega_i, \omega_o) = \frac{\sum_{f \in H_{\mathbf{x}}} \rho_f(\mathbf{n}_f, \omega_i, \omega_o) \gamma_f(\omega_i, \omega_o)(\mathbf{n}_f \cdot \omega_i)(\mathbf{n}_f \cdot \omega_o)}{A(H_{\mathbf{x}}, \omega_o)},$$
$$(2)$$

where f is a facet of $H_{\mathbf{x}}$ with normal $\mathbf{n}_f$ and rotated BRDF $\rho_f(\mathbf{n}_f, \omega_i, \omega_o)$, $A(H_{\mathbf{x}}, \omega_o)$ is the visible projected area of all facets in $H_{\mathbf{x}}$ along ω_o, and $\gamma_f(\omega_i, \omega_o)$ is the Bidirectional Facet Visibility Function (BFVF) that represents the visible area of f along both ω_i

and ω_o. Since the ink BRDFs are isotropic we simplify the above equation by dropping the tangent from the rotated BRDF ρ_f. We can write the projected visible area and BFVF as

$$A(H_{\mathbf{x}}, \omega_o) = \sum_f \int_{\mathbf{p} \in A(f)} V(\mathbf{p}, \omega_o)(\mathbf{n}_f \cdot \omega_o) \mathrm{d}\mathbf{p} \quad (3)$$

$$\gamma_f(\omega_i, \omega_o) = \int_{A(f)} V(\mathbf{p}, \omega_o) V(\mathbf{p}, \omega_i) \mathrm{d}\mathbf{p} \quad (4)$$

where $A(f)$ is the area of f and $V(\mathbf{p}, \omega_o)$ is a visibility function that is 1 if the facet point $\mathbf{p}$ is visible along ω_o and 0 otherwise. Please refer to the appendix for a detailed derivation of the effective BRDF of a bi-scale material.

From the previous equation we observe that the effective BRDF $\bar{\rho}(H_{\mathbf{x}}, \omega_i, \omega_o)$ of a bi-scale material patch $H_{\mathbf{x}}$ is determined by the normals $\mathbf{n}_f$, the isotropic BRDFs ρ_f and BFVFs γ_f of all facets f of $H_{\mathbf{x}}$. The facet normal can be computed from the heights of the facet's three vertices, while the BFVF of a facet is determined by the shape of the surrounding height field. Given the effective BRDF $\bar{\rho}$ of $H_{\mathbf{x}}$, we can compute the reflected radiance of the patch as

$$\bar{L}(H_{\mathbf{x}}, \omega_o) = \int_{\Omega} \bar{\rho}(H_{\mathbf{x}}, \omega_i, \omega_o) L_i(\omega_i) \mathrm{d}\omega_i. \quad (5)$$

Here the cosine factor of ω_i is embedded in the effective BRDF. In our system we fabricate the patches $H_{\mathbf{x}}$ such that the reflected radiance of each patch approximates the reflected radiance of the input appearance, i.e. $\bar{L}(H_{\mathbf{x}}, \omega_o) \approx L(\mathbf{x}, \omega_o)$ for all $\mathbf{x}$. We assume that the height field of the resulting bi-scale material is also defined on the XY plane. The bi-scale patch $H_{\mathbf{x}}$ at each input location $\mathbf{x}$ contains $N_f = 2N_h^2$ facets defined by $(N_h + 1)^2$ height samples, where N_h is the patch resolution. This results in a full height field of $N_x \cdot (N_h + 1) \times N_y \cdot (N_h + 1)$ resolution. In our current implementation, we use a patch resolution of $N_h = 5$ resulting in 50 facets for each patch.

BRDFs of ink combinations We model the BRDF ρ_c of each valid ink combination c as non-negative linear combination of N_m isotropic basis BRDFs $\{\hat{\rho}_1 \cdots \hat{\rho}_{N_m}\}$ and their weights $W_c = \{w_1 \cdots w_{N_m}, w_i \geq 0.0\}$, which is represented by $\rho_c = \sum_{w_i \in W_c} w_i \hat{\rho}_i$. In this representation, we constrain the sum of weights to be less than 1.0, $\sum_{w_i \in W_c} w_i \leq 1.0$. Therefore, the BRDF of each facet with ink combination c_f can be written as

$$\rho_f(n_f, \omega_i, \omega_o) = \sum_{w_i \in W_{c_f}} w_i \hat{\rho}_i(\mathbf{n}_f, \omega_i, \omega_o), \quad (6)$$

where $\hat{\rho}_i(\mathbf{n}_f, \omega_i, \omega_o)$ is the ink basis BRDFs rotated with normal $\mathbf{n}_f$, and W_{c_f} is the BRDF weights of ink combination c_f. We use this facet BRDF representation in our optimization.

To model the BRDF gamut of ink combinations, we first capture the BRDFs of all ink combinations as in [Dong et al. 2012] and then compute the BRDF basis and their linear weights for each BRDF in the gamut using the method in [Lawrence et al. 2006]. After that, we build a lookup table for all ink combinations and the weight of its BRDFs. Given the linear weights of basis BRDFs solved for each facet, we search the look-up table and find the printing weights that are closest to the desired weights and use the corresponding ink combination for printing. In our implementation, the basis BRDFs are represented by the isotropic Cook-Torrance model and we set $N_m = 6$, which faithfully represents the BRDFs of all ink combinations. The implementation details on the first capturing step for the BRDFs of all ink combinations are discussed in Section 5.
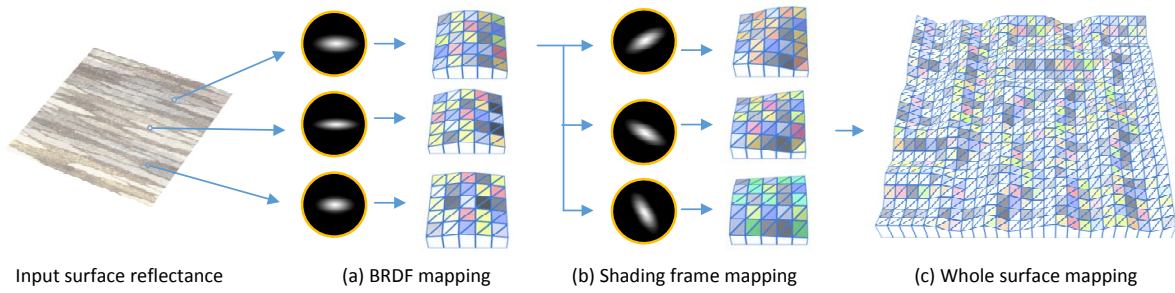
Figure 3: *The three steps of bi-scale mapping. (a) BRDF mapping. Starting from an input surface reflectance with per-point normal and tangent directions, our method first computes a bi-scale material patch that best matches the unrotated input BRDF at each individual point. (b) Shading frame mapping. A bi-scale material patch that best matches the input BRDF rotated with its shading frame is computed for each point. (c) Whole surface mapping. We tile the bi-scale material patches of all input samples together and optimize whole bi-scale material to generate the final result. The input BRDF is illustrated by a 2D slice sampled with the top view and all lighting directions.*

4   Bi-scale Mapping

Taking into account the manufacturing constraints, namely the patch resolution N_h and the BRDFs of the printable ink combinations, we determine the height field h and the facets' BRDF weights by minimizing the difference E between the input surface reflectance $\rho(\mathbf{n_x}, \mathbf{t_x}, \mathbf{x}, \omega_i, \omega_o)$ and the effective reflectance $\bar{\rho}(H_\mathbf{x}, \omega_i, \omega_o)$ of the resulting bi-scale material. We define this difference as

$$E = \int_\mathbf{x} \int_{\Omega \times \Omega} d(\rho(\mathbf{n_x}, \mathbf{t_x}, \mathbf{x}, \omega_i, \omega_o), \bar{\rho}(H_\mathbf{x}, \omega_i, \omega_o)) \mathrm{d}\omega_i \mathrm{d}\omega_o \mathrm{d}\mathbf{x} \quad (7)$$

where $\Omega \times \Omega$ is the bidirectional domain of ω_i and ω_o and d is the distance between two BRDFs that we compute as in [Ngan et al. 2005]. Note that the cosine factor for the effective BRDFs has been embedded in it. We call this optimization process *bi-scale mapping*.

This optimization problem is particularly challenging for two reasons. First, the effective BRDF is non-linearly related to the parameters we want to estimate. A good initialization is important for this non-linear optimization. However, finding a good initial height field remains difficult, especially in the case of rotated BRDFs. Second, since the effective BRDF at a location depends on the neighboring patches, the parameters of all patches need to be optimized together. As a result, the number of the estimated parameters is large. There are $N_x \times N_y \times (N_h + 1)^2$ unknowns for normals and $N_x \times N_y \times N_f \times N_m$ unknowns for facet BRDFs, resulting in over $3 \cdot 10^6$ parameters for a simple 100×100 input. These observations suggest that our optimization problem cannot be handled directly with standard non-linear optimization methods.

To address the underlying computational complexity, we solve the problem in three steps, as shown in Figure 3. At each step, we simplify the problem by solving for a smaller number of parameters while fixing the others. The solution of each step is used as the initialization of the next step providing a good initial solution that leads to fast convergence of the non-linear solver. We begin by ignoring the local shading frames and compute a bi-scale material that best matches the unrotated BRDFs. We then take the shading frames into consideration and compute the bi-scale material that best matches the rotated BRDFs, starting by rotating the patches obtained in the previous step. In the first two steps, we optimize each patch independently, effectively solving a large number of small non-linear optimizations, rather than a large one. In the last step, we tile the per-location patches computed independently into a whole surface and optimize the boundaries of neighboring patches and their BRDFs to obtain the final solution.
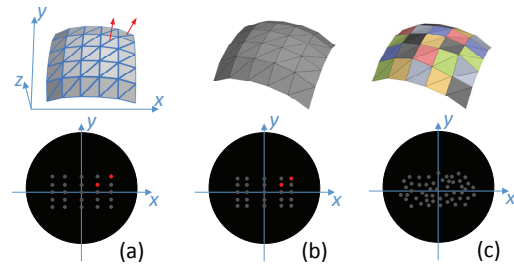
Figure 4: *Initialization. (a) By assuming each height field quad lies in the same plane and the patch shape is symmetric and convex, the facet normals form an axis-aligned grid in the angular domain and thus is determined by two normals (marked in red) for a 6×6 height field. (b) The initial height field for a bi-scale material patch. (c) The optimized height field of the bi-scale material patch.*

4.1   BRDF Mapping

For each location independently, we compute the $(N_h + 1)^2$ height values and $N_f \cdot N_m$ ink weights of the patch $H_\mathbf{x}^\rho$ that minimize the difference $E_\mathbf{x}^\rho$ between the patch's effective BRDF $\bar{\rho}(H_\mathbf{x}^\rho, \omega_i, \omega_o)$ and the unrotated input BRDF $\rho(\mathbf{x}, \omega_i, \omega_o)$. Here we ignore the rotations induced by the local shading frames and regard the input BRDFs as defined in the global coordinate system. We use the superscripts E^ρ and H^ρ to indicate that. With this notation, we can write the error at a surface location as

$$E_\mathbf{x}^\rho = \int_{\Omega \times \Omega} d(\rho(\mathbf{x}, \omega_i, \omega_o), \bar{\rho}(H_\mathbf{x}^\rho, \omega_i, \omega_o)) \mathrm{d}\omega_i \mathrm{d}\omega_o. \quad (8)$$

At each surface location, this leads to solving a reasonably small non-linear optimization problem that can be tackled with a good initial estimate.

Initialization   To simplify the initialization, we ignore shadowing and masking effects and assume all facets share one unknown isotropic BRDF. Thus we can compute the initial facet normals of the height field by minimizing a simplified version of Equation 8 and constraining the integrability of resulting normals to ensure they form a valid height field. This still requires a non-linear optimization that is challenging due to the large solution space.

To solve this issue, we further simplify the optimization by imposing constraints on the facet normals, namely that each pair of triangles that correspond to a height field quad lie in the same plane. As shown in Figure 4.a, this constraint leads to the quad normals of a valid height field forming an axis-aligned grid in the angular domain. This not only greatly reduces the number of unknowns
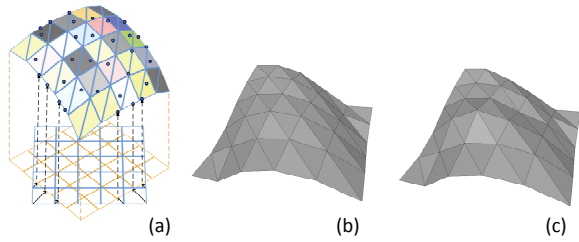
Figure 5: *Shading frame mapping. (a) The bi-scale material patch obtained in the last step is rotated back to its shading frame and resampled by the regular grid of the height field (shown in blue). (b) The resampled height field patch. (c) The height field patch after optimization.*

(a) Boundary facets (b) Updates boundary in 2x2 region (c) Before optimization (d) After optimization

(e) Input surface appearance (f) Before optimization (g) After optimization
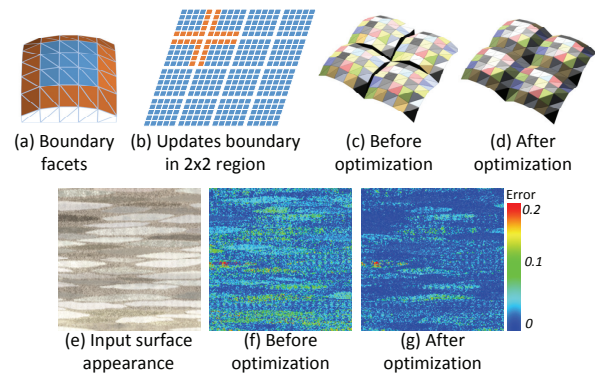
Figure 6: *Whole surface mapping. (a) For each patch, we fix its central part (shown in blue) and only update the height and BRDF weights of the patch boundaries (shown in brown) by global optimization. (b) In each step, we update the height and BRDF weights of 2×2 patch boundaries (shown in red). For the input appearance shown in (e), (f) and (g) show the error maps of the bi-scale mapping result before and after the whole surface mapping, the patch boundaries before and after optimization are also illustrated in (c) and (d).*

for the facet normals from $2 \times N_h^2$ to $2 \times N_h$, but also guarantees that the resulting facets form a valid height field, so we do not need to explicitly impose constraints for integrability of the normal field. Moreover, since most BRDFs are symmetric along the tangent and bi-tangent directions [Holroyd et al. 2008], for each patch we seek symmetric pyramid-like height fields centered along the main surface normal. This constraint further reduces the number of unknowns for the facet normals from $2 \times N_h$ to $N_h/2$ unknowns.

Based on these two constraints, we initialize the BRDF of the patch as the average BRDF of all ink combinations and update both normals and BRDF weights with a gradient based method [Nocedal 1980]. Figure 4.b illustrates the initial height field and their facet normals.

Iterative Optimization   Given the initial height field and BRDF weights, we iteratively optimize the BRDF weights of each facet and the unconstrained height field locations by minimizing the error $E_{\mathbf{x}}^{\rho}$ from Equation 8. All the constraints imposed during initialization are removed in this step. As a result, the normals and BRDFs of facets can be different while the shadowing and masking effects between facets (BFVF) are also considered in this step. At each iteration, we first fix the height field and BFVF and optimize the BRDFs. This can be formulated as a non-negative least squares problem that we solve by quadratic programming. We then fix the BRDF weights and optimize the height field with a gradient-based method [Nocedal 1980]. We continue iterating until convergence or the error reduction between two steps is lower than a user-specified threshold, in our case set to 0.01. In this iterative optimization, we compute the BFVF of the height field with the method in [Wu et al. 2011]. Figure 4 shows the height field patch and its facet normals after iterative optimization.

Subsampling   To further speed up the mapping, we cluster the unrotated input BRDFs of all pixels and solve the BRDF mapping only for the representative BRDF of each cluster. In practice, we use k-means clustering and progressively add cluster numbers until the difference between any two BRDF samples within a cluster is smaller than 0.01. After that, we do BRDF mapping for the representative BRDF of each cluster. Then for each BRDF in the cluster, we use the bi-scale patch of the representative BRDF for initialization. Finally we optimize the patch for each BRDF with the iterative optimization method mentioned above. This greatly speeds up the BRDF mapping process.

4.2 Shading Frame Mapping

In this step, we take the shading frames into account and compute the bi-scale patch $H_{\mathbf{x}}$ for each rotated BRDF $\rho(\mathbf{n_x}, \mathbf{t_x}, \mathbf{x}, \omega_i, \omega_o)$

by minimizing the difference E between its effective BRDF $\bar{\rho}(H_{\mathbf{x}}, \omega_i, \omega_o)$ and the input surface reflectance $\rho(\mathbf{n_x}, \mathbf{t_x}, \mathbf{x}, \omega_i, \omega_o)$, where E can be written as

$$E_{\mathbf{x}} = \int_{\Omega \times \Omega} (\rho(\mathbf{n_x}, \mathbf{t_x}, \mathbf{x}, \omega_i, \omega_o)(\mathbf{n_x} \cdot \omega_i) - \bar{\rho}(H_{\mathbf{x}}, \omega_i, \omega_o))^2 \mathrm{d}\omega_i \mathrm{d}\omega_o.$$
(9)

However, we cannot follow the initialization method in the first step of this optimization. Although the symmetric pyramid height field provides a good initial estimate for unrotated BRDFs, it cannot model rotated BRDFs with arbitrary tangents and normals. We ths initialize the height field with the rotated bi-scale patch $H_{\mathbf{x}}^{\rho}$ obtained in the last step. As shown in Figure 5, we rotate $H_{\mathbf{x}}^{\rho}$ to its local shading frame and resample it to $H_{\mathbf{x}}$ with the axis-aligned grid of $H_{\mathbf{x}}$. For grid points that are out of the patch region projected on the XY plane, we find its nearest point on the patch region and sample its height value for initialization. After that, we iteratively optimize the BRDF weights and height field using the same iterative solver described in the first step. Conceptually, the only difference is that in this optimization we minimize $E_{\mathbf{x}}$ instead of $E_{\mathbf{x}}^{\rho}$ in this step.

4.3 Whole Surface Mapping

The above two steps compute the optimal bi-scale patch for each surface location individually. However, we cannot obtain the optimal bi-scale material surface for the input surface reflectance by simply tiling the optimal patches together. Discontinuities and non-integrable normals along the patch boundaries lead to difficulties during fabrication, while the shadowing and masking effects between different patches affect the appearance of each patch. To solve these two issues, we tile all patches together and optimize the whole height field and BRDFs by minimizing the difference between the input surface reflectance and the effective reflectance of the resulting bi-scale material defined in Equation 7. Since each bi-scale patch obtained in the last two steps is optimal for the input surface reflectance at a single location, we fix the height values and BRDF weights of the internal facets of each patch and only optimize the height values and BRDF weights of facets on the patch boundaries (shown in Figure 6.a). Although this strategy reduces the number of estimated parameters, the number of height values

and BRDF weights on the patch boundaries is still large and cannot be directly computed with standard non-linear optimization methods. We address this issue by iteratively optimizing a subset of the parameters while fixing others. We initialize the height value of a patch boundary with the average height of neighboring patches that border the boundary point. As shown in Figure 6.b, we then update the height values and BRDF weights for boundaries shared by 2×2 patches and fix all others in each step. We repeat this step for all 2×2 patches and thus update all height values and BRDF weights on patch boundaries. We iterate the whole process several times until the error difference between two iterations is smaller than a user specified threshold (0.001 in our implementation). As shown in Figure 6.e, our whole surface mapping can further improve the results by solving the optimal continuous height map, thus reducing unwanted shadowing and masking effects.

5   Hardware Setup

Since we found no commercial hardware that could simultaneously fabricate the height field and deposit the glossy inks, we print our bi-scale material in three steps shown in Figure 7 for the input reflectance of Figure 1. We first fabricate the height field using a 3D printer (Figure 7.a). We then coat it with metallic paint to obtain a constant glossy finish (Figure 7.b). We finally print the desired BRDFs over the surface using a flatbed color printer (Figure 7.c).

Height Field Fabrication   We use an Objet Eden 500V to print the height field. This hardware has a printing resolution of $600 \times 600 \times 1600$ DPIs and a maximum object size of $500 \times 400 \times 200$ mm. In our experiments we use patches of 6×6 resolution. We set the grid interval to be $0.14mm$ corresponding to patches of 0.7×0.7 mm^2 surface area. We print the height field over a 7 mm thick block to improve its robustness.

BRDF Printing   We print the BRDFs over the height field with an Océ Arizona 318 GL UV flatbed printer that supports the Process Metallic Color System. As shown in Figure 7.d, this device consists of a printing head that moves along the X and Y directions while the printable material lies on a fixed flatbed. The printer has a resolution of 1440 DPI with 8-bit depth for each channel and can print over an object surface whose height variation is smaller than 48 mm. This allows us to print an ink combination for each height field facet. We vary surface color by printing UV curable CMYK inks. To obtain variable glossiness, we first coat the whole height field with a homogeneous silver metallic paint (Mr.Hobby GSI-SM08). We then print UV curable diffuse white ink onto the metallic coating to control the glossiness of each pixel. During printing we assume that the coating has no spatial variation.

Printer Registration   Since the height field and BRDFs are printed by two separate devices, we need to register the BRDF printer to the underlying height field. We assume that the motion of the color printer head is accurate and perform registration by determining the necessary translation and orientation of the height field. In our current implementation, we found that the rotation between the height field and BRDF print is small and can be ignored safely. We thus construct a Vernier scale with the main geometry scale and sliding secondary color scale for computing the translation of the height field. Specifically, After fabricating the geometry scale pattern along both sides of the resulting height field, we manually place the printed 3D block on the flatbed and print the color scale pattern over the geometry scale pattern. As shown in Figure 7.e, the interval of the color scale is ten image pixels while the interval of the geometry scale is eleven image pixels. When the n-th pattern of the two scales are aligned, the offset between the two patterns (i.e. the offset between the BRDF print and the underlying height field) is n pixels. With the geometry scale pattern along both sides of the 3D block, we can calculate the 2D translations between color

Datasets	Resolution	Mapping Time (m)	Fitting Error	A.	F.	M.
IST Wallpaper	140×140	70	7.35%	Y	Y	Y
Wallpaper II	200×200	70	12.37%	Y	Y	Y
Yellow Satin	215×215	75	10.68%	Y	Y	Y
Red Satin	212×212	80	15.73%	Y	Y	Y
RustMetal	140×140	55	9.62%	N	Y	N
Wood	120×120	60	11.34%	N	Y	H

Table 1: *The input dataset properties, including whether they are anisotropic (A), have local frames (F) and are measured (M). For the latter, we indicate with H when only the local frame was measured.*

printing and the underlying height field. After that, we translate the ink combination image contents accordingly and print the desired ink combinations onto the height field. Although this method has limited resolution, it works well for our application.

BRDF Gamut Measurement   To compute the bi-scale material, we need to measure the BRDFs of all valid ink combinations. We follow [Dong et al. 2012] and reconstruct the BRDFs of all ink combinations by measuring the BRDFs of a densely sampled subset of combinations and interpolating the rest. In particular, we uniformly sampled 8 levels for each of the RGB color channels and the white ink channel. We tiled the resulting 4096 ink combinations in a 1280×1280 image with a 20×20 patch for each ink combination and printed all tiles onto a flat $10cm \times 10cm$ surface coated with the metallic paint. We then captured the BRDFs of all surface points by linear light source reflectometry [Gardner et al. 2003] and average the BRDFs in each tile by computing the BRDF of the corresponding ink combination. The BRDFs of all other ink combinations are then computed as the locally linear combinations of BRDFs of the sampled ink combinations. For an ink combination $c = \sum_{k=1}^{K} w_k c_k$, its BRDF ρ_c is modeled by $\rho_c = \sum_{k=1}^{K} w_k \rho_{c_k}$, where ρ_{c_k} are BRDFs of the sampled ink combinations c_k in a local neighborhood of size $K = 5$. After we get the BRDFs of all ink combinations, we compute the basis and linear weights of all BRDFs as described in Section 3.

6   Experimental Results

We evaluated our method by fabricating measured and designed appearance datasets that exhibit different scattering characteristics. For all results shown, one pixel of the measured data corresponds to a 0.7×0.7 mm^2 patch in fabrication, thus the physical size is solely determined by the dataset resolution.

Performance   We tested our bi-scale material mapping algorithm on an Intel Xeon E5400 CPU and 8GB memory. The algorithm is executed in a single thread and takes around 50 to 80 minutes for a 400×400 input reflectance. The timing is dominated by BRDF fitting that takes 30 to 60 minutes depending on the SVBRDFs complexity. The remaining time is mostly spent in local frame fitting, with the final optimization taking roughly 2 minutes. Table 1 lists the properties of all datasets and the computation times for the material mapping. For all the input datasets and during our optimization, we uniformly sampled the angular domain of BRDFs using θ, ϕ coordinates, with $10 \times 40 \times 10 \times 40$ samples for $\omega_i(\theta, \phi)$ and $\omega_o(\theta, \phi)$, for a total of $160K$ samples per BRDF.

Validation   We quantitatively analyzed the accuracy of our bi-scale mapping algorithm for all input datasets by computing the relative error, based on [Ngan et al. 2005], between the input surface reflectance and the predicted output bi-scale appearance. The results are listed in Table 1. With an error of roughly 10% on aver-
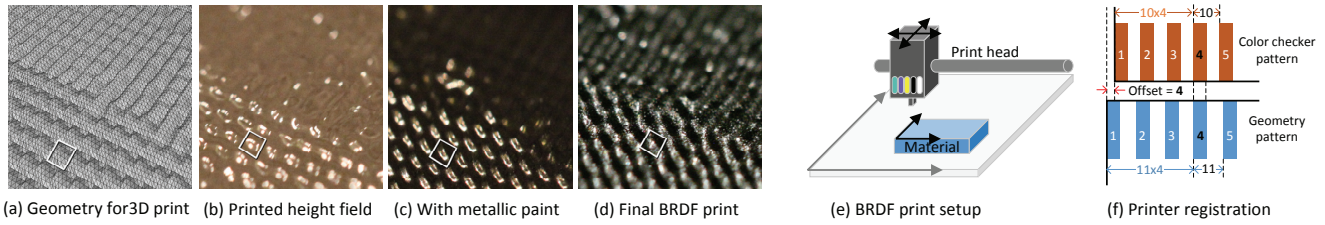
| (a) Geometry for 3D print | (b) Printed height field | (c) With metallic paint | (d) Final BRDF print | (e) BRDF print setup | (f) Printer registration |

Figure 7: *Hardware setup. (a) The height field generated by bi-scale mapping, which is the input for the 3D print. (b) The height field fabricated by a 3D printer. (c) The height field coated with homogeneous metallic paint. (d) The final result covered by the glossy inks. A single bi-scale patch that corresponds to an input surface reflectance sample is marked with white rectangles. (e) An illustration of the BRDF print setup. (f) An illustration of the Vernier scale used for printer registration. When the 4th patterns of the two scales are aligned, the offset (4 pixels) between the two scales is the difference between the length of four color pattern intervals and the length of four geometry pattern intervals.*
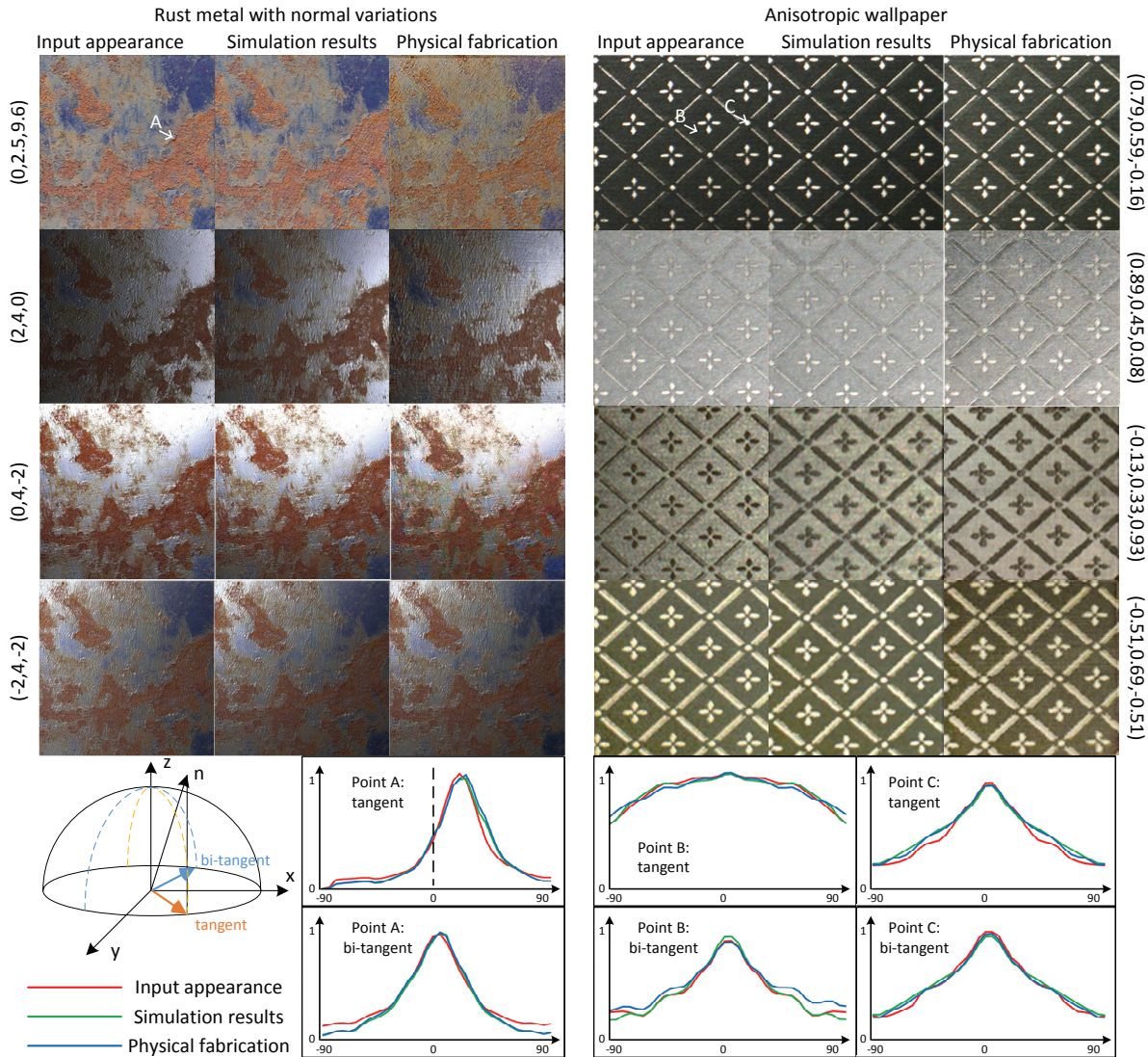
Figure 8: *Method validation. The top four rows compare the input surface appearance, our simulation results and photographs of the fabricated results under different lightings. The viewing direction is fixed and the point light position for the results in each row is listed on the side. The left columns show results for the rust metal dataset, while the right ones show results for the IST wallpaper dataset. The bottom two rows plot the angular responses of input reflectance for three points (marked as A, B and C) and the responses of their corresponding bi-scale patches. The response curves are rendered and measured with a fixed top view and a point light source moving along the arc in the plane determined by the normal and tangent direction and the arc in the plane determined by the normal and bi-tangent direction. Note that the specular peak of point A is shifted towards the normal direction, while the anisotropic reflectance of point B produces very different responses along different directions. All these BRDFs are well reproduced by the fabrication results.*
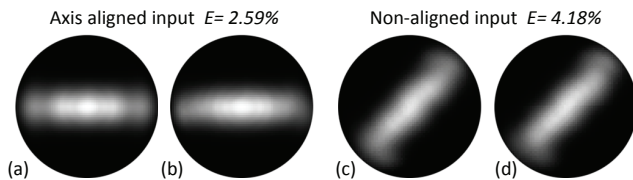
Figure 9: *Method validation with known bi-scale materials. We manually generate two bi-scale materials with different tangent directions. With their BRDFs (a) and (c) as input, the resulting bi-scale patches generated by our bi-scale mapping exhibit similar BRDFs shown in (b) and (d). Each image shows a 2D slice of the BRDF under a fixed top view and all lighting directions. The mapping errors of the two results are also listed.*

Figure 10: *The printing gamut. The solid orange line plots the isotropic BRDF gamut of ink combinations. The light blue region indicates the printing gamut of bi-scale material patches with a 6 × 6 height field covered by ink combinations. The dark blue region illustrates the printing gamut of bi-scale material patches with a single homogeneous BRDF (marked as D). C indicates the BRDF with the largest anisotropic ratio in our printing gamut. Note that our method extends both the isotropic and anisotropic printing gamut by combining the isotropic BRDFs of ink combinations and a small scale height field.*

age, our method reproduces very well the input appearance with an ink set not designed for these cases.

To test the fidelity in reproducing different BRDFs, we fabricated the wallpaper dataset from [Lawrence et al. 2006] since it has both anisotropic BRDFs as well as high-gloss isotropic ones. We tested the reproduction of geometric details by fabricating a rusted metal dataset from [Dong et al. 2011], which has rich normal variations and spatially-varying isotropic reflectance. The top four rows of Figure 8 shows renderings for both the input appearance and the output bi-scale surface, together with photographs of the fabricated objects. For each input sample, the rendering and photograph taken under the same local point light source are shown in the same row, while the images in different rows illustrate the results lit with point lights at different positions. The photographs are taken with a calibrated lighting and camera that match the rendered images. As shown by these images, our fabrication results can reproduce well the complex input surface appearance. In the bottom two rows of Figure 8, we also quantitatively analyze the accuracy of our fabricated results by plotting the appearances of three points in the input surface reflectance (shown in red) and their appearances in both the bi-scale surface patch (shown in green) and fabrication results (shown in blue). For all three samples, we capture their appearances under the fixed top view and point lights moving along the 1D arcs. As shown in Figure 8, the appearances of the fabricated samples are similar to the rendered appearances of the input and its corresponding bi-scale surface patch.

We also validated the bi-scale mapping algorithm with two bi-scale materials with different local frames, both of which are synthesized with 6 × 6 height fields and ink BRDFs. The BRDFs of two materials are then used as the input of the bi-scale mapping. As shown in Figure 9, the BRDFs of the bi-scale mapping results are similar to the inputs, and the relative errors between the input and output BRDFs are 2.59% and 4.18% respectively.

Complex Reflectance   Figure 12 and 13 illustrate two fabricated textiles with strong anisotropic behavior measured from real samples [Wang et al. 2008]. One method is capable of reproducing both the strong anisotropy and rich color details when viewed under different lighting directions. Figure 14 shows the printing result of another wallpaper dataset from [Wang et al. 2008], which exhibits complex tangent variations. Note that our method well captures the interaction between anisotropy and local frame rotations and reproduces its appearance variations under different lighting and viewing conditions. We also fabricated wood data with a measured normal map [Toler-Franklin et al. 2007] and the spatially varying reflectance obtained from [Dong et al. 2011]. As shown inFigure 15, our result exhibits realistic appearance resulting from the combination of BRDF variations and surface details. Note that the appearance variations caused by the non-integrable normals in this
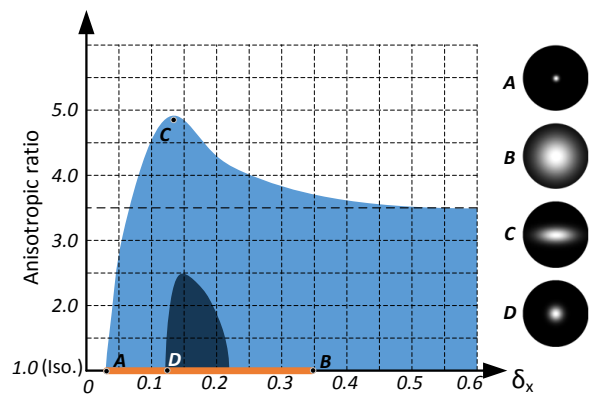
dataset are well reproduced by our method, where the BRDF and normal at each input point are modeled by the higher resolution normal field of facets and their BRDFs.The inset images in all results show a closeup view of our fabricated results.

Our method can also work with a 3D printer for printing 3D objects with desired spatially varying surface appearance. Figure 16 illustrates a 3D teapot with designed surface appearance fabricated by our method. To this end, we mapped the bi-scale material of the IST wallpaper data to the teapot surface. We assume the curvature at each surface point is large enough compared to the size of the bi-scale patch so that the deformation of the mapped height field can be ignored. The teapot body surface is divided into four parts so that we can print the BRDFs over the surface with the flatbed UV printer. After each part is printed, we stitched them together. Note that the anisotropic effects on the teapot body create interesting lighting effects.

Printing Gamut   We evaluate the capability of the proposed printing system by plotting the gamut of printable anisotropic BRDFs in Figure 10. We plot the gamut in the space of microfacet BRDFs with anisotropic Gaussian NDFs. We examine the roughness range of 0.001 to 0.6 since such a range covers most anisotropic reflectance effects. In the figure, we indicate in blue the BRDFs that can be reproduced with error smaller than 5% using our inks and 5 × 5 facets, in black the BRDFs that can be reproduced by facets with a single homogeneous BRDF (marked as D), and in orange the BRDFs that can be reproduced by the isotropic inks alone. Note that by combining facet orientations and ink variations, our system produces a significantly larger gamut than using either inks or facets alone. Also note that our bi-scale material even extends the isotropic printing gamut by simulating rougher BRDFs with sharper specular inks used with different facet orientations.

Limitations   Our system has a few limitations. On the hardware side, the resolution and accuracy of the 3D printer are limited. As a result, we need to carefully choose the height field resolution for each input surface reflectance sample. Although a higher height field resolution can model the input surface reflectance better, it
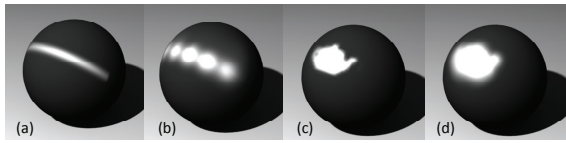
Figure 11: *Two failure cases of our method. (a) A BRDF with sharp specularity. (b) The bi-scale mapping result for the BRDF in (a). (c) A BRDF with complicated specular reflectance. (d) The bi-scale mapping result for the BRDF in (c). The homogeneous sphere in each image is mapped with the corresponding BRDF and rendered under a single point light.*

also leads to worse visual effects caused by the large patch size. For the hardware used in our implementation, the 5×5 height field for each bi-scale patch achieves the best trade-off between visual quality and representation capability. However, the facet of the bi-scale patch is still visible at a close view due to the limited resolution of 3D printers. Also, the fabricated facets do not exactly match the designed height field due to the limited accuracy of the 3D printer. The BRDF of the diffuse ink used by the color printer is glossy, which prevents our method from reproducing diffuse BRDFs. Furthermore, we have noticed that some ink combinations exhibit minor translucency which we do not account for.

On the fabrication process side, our main limitation is the need for a two step fabrication process that limits both the smallest possible facet size, to avoid registration issues, and the maximum height of the printed object, due to the use of a flatbed printer. Since recent 3D printers have multiple nozzles for printing in color, we believe that in the future it should be possible to adapt that technology and directly coat object surfaces with inks similar to ours while the height field is fabricated. One way to ameliorate this issue is to fabricate surfaces in plates that are then assembled in 3D. We have done just that in Figure 16. Another concern stems from imperfection in the metallic coating that can affect both geometry and BRDFs over the facet and thus decrease the final printing quality. We believe this could also be easily avoided with an integrated hardware solution.

On the bi-scale mapping side, the regular triangulation of the height field may cause some bias for anisotropic BRDFs with different tangent directions. In practice, we have not found any significant bias in our current print results. This is because a 5×5 patch is more effective for modeling anisotropic BRDF with different tangent rotations than a lower resolution patch. The varying BRDFs used for different patch facets also ameliorate this issue. We believe that other triangulation schemes such as the one used in [Alexa and Matusik 2010] could provide a better solution for shading frame mapping but we leave this for future work.

Finally, our material model ignores facet interreflections that might induce a smaller gamut. While these effects are minor in our printed example, future work should address these issues by extending the bi-scale model to include both interreflections and translucency.

With these hardware and software limitations, our method cannot well reproduce BRDFs with sharper specularity or anisotropic BRDFs with rich details. Figure 11 illustrates the two failure cases of our method.

7 Conclusion

We have presented an efficient method for printing custom surface appearance with anisotropic reflectance and shading frame variations. Our method models the input surface appearance at each point with the average appearance of a bi-scale material that consists of a small scale height field with printed glossy BRDFs over each facet. An optimization algorithm has been proposed to auto-

matically construct the bi-scale material from the input SVBRDFs and per-point shading frames. We fabricate the resulting height field with a 3D printer and subsequently print the BRDFs over the facets with a flatbed UV printer. Experimental results show that even with simple isotropic BRDFs for the inks and a low resolution height field for each surface patch, our method can reproduce well a wide range of surface appearance with different characteristics of spatial variations and anisotropic properties.

For future work, we would like to improve our bi-scale material model by taking inter-reflections between the facets into consideration so that we can better predict the appearance of the fabricated result. Also, we would like to consider other BRDF distance metrics (e.g. the one in [Pereira and Rusinkiewicz 2012]) in our optimization framework. Finally, it would be interesting to develop a unified and efficient hardware solution for directly printing the height field and BRDFs over the 3D object surface in a single pass.

Acknowledgements

References

ALEXA, M., AND MATUSIK, W. 2010. Reliefs as images. *ACM Trans. Graph. 29*, 4 (July), 60:1–60:7.

ASHIKMIN, M., PREMOŽE, S., AND SHIRLEY, P. 2000. A microfacet-based brdf generator. In *Proceedings of the 27th annual conference on Computer graphics and interactive techniques*, ACM Press/Addison-Wesley Publishing Co., New York, NY, USA, SIGGRAPH '00, 65–74.

BERMANO, A., BARAN, I., ALEXA, M., AND MATUSK, W. 2012. Shadowpix: Multiple images from self shadowing. *Comp. Graph. Forum 31*, 2 (May), 593–602.

DONG, Y., WANG, J., PELLACINI, F., TONG, X., AND GUO, B. 2010. Fabricating spatially-varying subsurface scattering. *ACM Trans. Graph. 29* (July), 62:1–62:10.

DONG, Y., TONG, X., PELLACINI, F., AND GUO, B. 2011. Appgen: interactive material modeling from a single image. ACM, New York, NY, USA, vol. 30, 146:1–146:10.

DONG, Y., TONG, X., PELLACINI, F., AND GUO, B. 2012. Printing spatially-varying reflectance for reproducing hdr images. *ACM Trans. Graph. 31*, 4 (July), 40:1–40:7.

DORSEY, J., RUSHMEIER, H., AND SILLION, F. 2008. *Digital Modeling of Material Appearance*. Morgan Kaufmann Publishers Inc., San Francisco, CA, USA.

GARDNER, A., TCHOU, C., HAWKINS, T., AND DEBEVEC, P. 2003. Linear light source reflectometry. *ACM Trans. Graph. 22*, 3 (July), 749–758.

GONDEK, J. S., MEYER, G. W., AND NEWMAN, J. G. 1994. Wavelength dependent reflectance functions. In *Proceedings of the 21st annual conference on Computer graphics and interactive techniques*, ACM, New York, NY, USA, SIGGRAPH '94, 213–220.
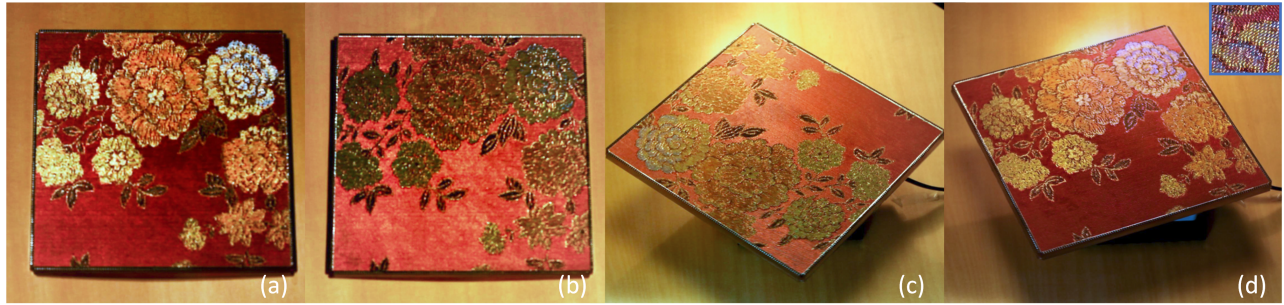
Figure 12: *Photographs of fabricated anisotropic yellow stain. (a)(b) lit with directional lighting. (c)(d) lit with environmental lighting.*
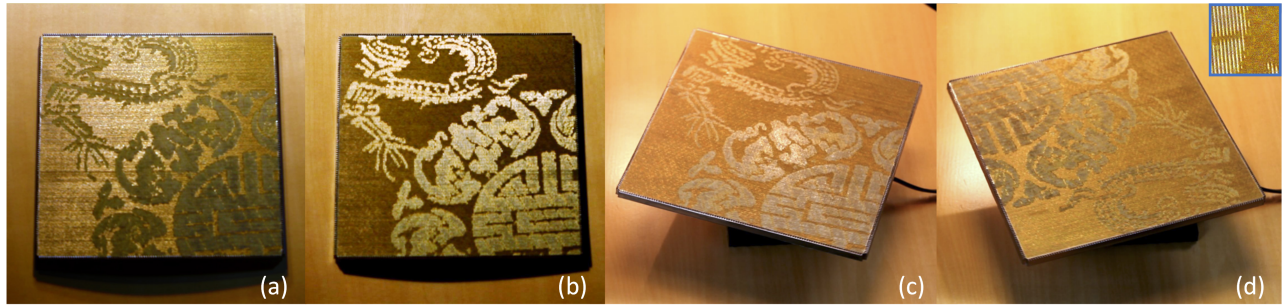

Figure 13: *Photographs of fabricated anisotropic red stain. (a)(b) lit with directional lighting. (c)(d) lit with environmental lighting. The rich color variations and anisotropic reflectance of the input sample are well reproduced by the fabricated result.*
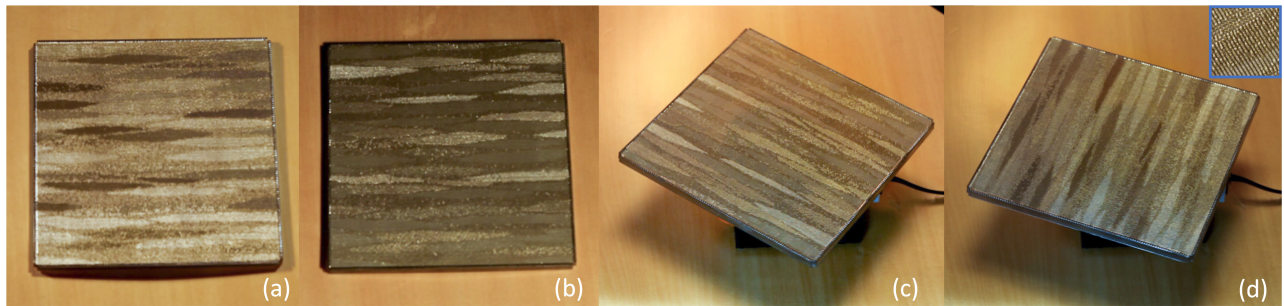

Figure 14: *Photographs of the fabricated result for the anisotropic wallpaper data. (a)(b) lit with directional lighting. (c)(d) lit with environmental lighting.*
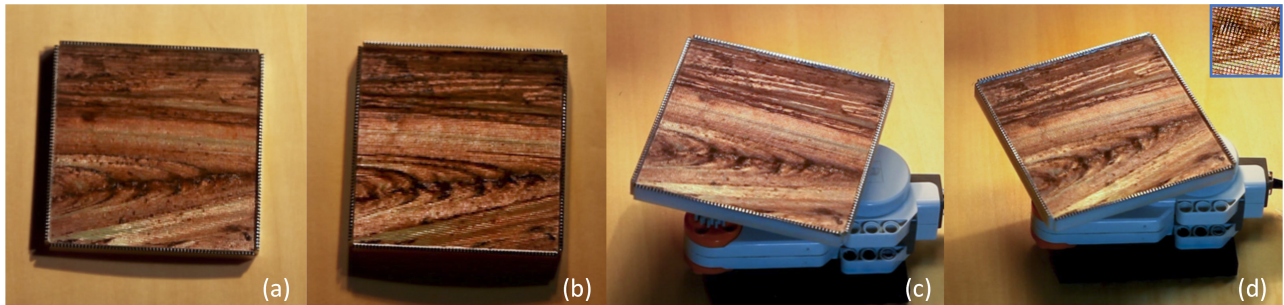

Figure 15: *Photographs of the fabricated result for the wood dataset. The detailed normal variations of the input are well printed. (a)(b) lit with directional lighting. (c)(d) lit with environmental lighting.*
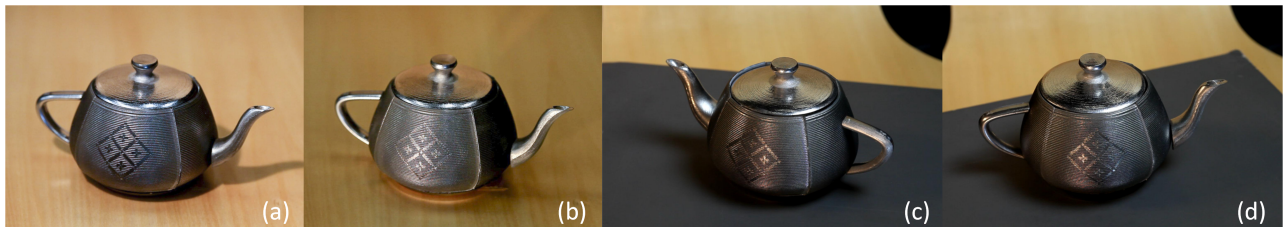

Figure 16: *Photographs of a 3D teapot. The 3D shape is printed by a 3D printer while the surface appearance is fabricated by our method. (a)(b) lit with directional lighting. (c)(d) lit with environmental lighting.*

HAŠAN, M., FUCHS, M., MATUSIK, W., PFISTER, H., AND RUSINKIEWICZ, S. 2010. Physical reproduction of materials with specified subsurface scattering. *ACM Trans. Graph. 29* (July), 61:1–61:10.

HEIDRICH, W., DAUBERT, K., KAUTZ, J., AND SEIDEL, H.-P. 2000. Illuminating micro geometry based on precomputed visibility. In *Proceedings of the 27th annual conference on Computer graphics and interactive techniques*, ACM Press/Addison-Wesley Publishing Co., New York, NY, USA, SIGGRAPH '00, 455–464.

HOLROYD, M., LAWRENCE, J., HUMPHREYS, G., AND ZICKLER, T. 2008. A photometric approach for estimating normals and tangents. *ACM Trans. Graph. 27*, 5 (Dec.), 133:1–133:9.

HOLROYD, M., BARAN, I., LAWRENCE, J., AND MATUSIK, W. 2011. Computing and fabricating multilayer models. *ACM Trans. Graph. 30* (Dec.), 187:1–187:8.

HULLIN, M. B., LENSCH, HENDRIK P. A.AND RASKAR, R., SEIDEL, H.-P., AND IHRKE, I. 2011. Dynamic display of BRDFs. In *Computer Graphics Forum (Proc. EUROGRAPHICS)*, Blackwell, Llandudno, UK, O. Deussen and M. Chen, Eds., Eurographics, 475–483.

IWASAKI, K., DOBASHI, Y., AND NISHITA, T. 2012. Interactive bi-scale editing of highly glossy materials. *ACM Trans. Graph. 31*, 6 (Nov.), 144:1–144:7.

LAWRENCE, J., BEN-ARTZI, A., DECORO, C., MATUSIK, W., PFISTER, H., RAMAMOORTHI, R., AND RUSINKIEWICZ, S. 2006. Inverse shade trees for non-parametric material representation and editing. *ACM Trans. Graph. 25*, 3 (July), 735–745.

MALZBENDER, T., SAMADANI, R., SCHER, S., CRUME, A., DUNN, D., AND JAMES, D. 2012. Printing reflectance functions. *ACM Trans. Graph. 31*, 3 (June), 20:1–20:11.

MATUSIK, W., AJDIN, B., GU, J., LAWRENCE, J., LENSCH, H. P. A., PELLACINI, F., AND RUSINKIEWICZ, S. 2009. Printing spatially-varying reflectance. *ACM Trans. Graph 28* (December), 128:1–128:9.

NGAN, A., DURAND, F., AND MATUSIK, W. 2005. Experimental analysis of BRDF models. *Eurographics Symposium on Rendering 2005*, 117–226.

NOCEDAL, J. 1980. Updating Quasi-Newton Matrices with Limited Storage. *Mathematics of Computation 35*, 151, 773–782.

PAPAS, M., HOUIT, T., NOWROUZEZAHRAI, D., GROSS, M., AND JAROSZ, W. 2012. The magic lens: refractive steganography. *ACM Trans. Graph. 31*, 6 (Nov.), 186:1–186:10.

PEREIRA, T., AND RUSINKIEWICZ, S. 2012. Gamut mapping spatially varying reflectance with an improved BRDF similarity metric. *Computer Graphics Forum (Proc. Eurographics Symposium on Rendering) 31*, 4 (June).

REGG, C., RUSINKIEWICZ, S., MATUSIK, W., AND GROSS, M. 2010. Computational highlight holography. *ACM Trans. Graph. 29*, 6 (Dec.), 170:1–170:12.

TOLER-FRANKLIN, C., FINKELSTEIN, A., AND RUSINKIEWICZ, S. 2007. Illustration of complex real-world objects using images with normals. In *International Symposium on Non-Photorealistic Animation and Rendering (NPAR)*.

WANG, J., ZHAO, S., TONG, X., SNYDER, J., AND GUO, B. 2008. Modeling anisotropic surface reflectance with example-based microfacet synthesis. *ACM Trans. Graph. 27*, 3 (Aug.), 41:1—-41:9.

WESTIN, S. H., ARVO, J. R., AND TORRANCE, K. E. 1992. Predicting reflectance functions from complex surfaces. *SIGGRAPH Comput. Graph. 26*, 2 (July), 255–264.

WEYRICH, T., PEERS, P., MATUSIK, W., AND RUSINKIEWICZ, S. 2009. Fabricating microgeometry for custom surface reflectance. *ACM Trans. Graph. 28*, 3 (July), 32:1–32:6.

WU, H., DORSEY, J., AND RUSHMEIER, H. 2009. Characteristic point maps. In *Proceedings of the Twentieth Eurographics conference on Rendering*, Eurographics Association, Aire-la-Ville, Switzerland, Switzerland, EGSR'09, 1227–1236.

WU, H., DORSEY, J., AND RUSHMEIER, H. 2011. Physically-based interactive bi-scale material design. *ACM Trans. Graph. 30* (Dec.), 145:1–145:10.

ZHAO, S., JAKOB, W., MARSCHNER, S., AND BALA, K. 2011. Building volumetric appearance models of fabric using micro ct imaging. *ACM Trans. Graph. 30*, 4 (July), 44:1–44:10.

ZHAO, S., JAKOB, W., MARSCHNER, S., AND BALA, K. 2012. Structure-aware synthesis for predictive woven fabric appearance. *ACM Trans. Graph. 31*, 4 (July), 75:1–75:10.

Appendix

Effective BRDF of a Bi-scale Material

Here we provide a detailed derivation of the formula for the effective BRDF of a bi-scale material. The first several steps are similar to the derivations in [Wu et al. 2011]. Starting from the reflectance at single position $\mathbf{p}$ with the normal $\mathbf{n_p}$, BRDF ρ and visibility function $V(\mathbf{p}, \omega)$, the outgoing radiance L at position $\mathbf{p}$ along a view direction ω_o is:

$$L(\mathbf{p}, \omega_o) = \int_{\Omega} \rho(\mathbf{n_p}, \mathbf{p}, \omega_i, \omega_o) V(\mathbf{p}, \omega_i) L_i(\mathbf{p}, \omega_i)(\mathbf{n_p} \cdot \omega_i) d\omega_i \qquad (10)$$

The visibility function $V(\mathbf{p}, \omega)$ equals 0 if $\mathbf{p}$ is blocked in direction ω or equals 1 when $\mathbf{p}$ is visible. Then for one pixel of the bi-scale material $H(\mathbf{x})$, the averaged reflected radiance $\bar{L}$ at direction ω_o can be calculated by averaging all visible reflected radiance.

$$\bar{L}(H_{\mathbf{x}}, \omega_o) = \frac{1}{A(H_{\mathbf{x}}, \omega_o)} \int_{A_v(H_{\mathbf{x}}, \omega_o)} L(\mathbf{p}, \omega_o) d\mathbf{p} \qquad (11)$$

where $A(H_{\mathbf{x}}, \omega_o)$ is the visible projection area of $H_{\mathbf{x}}$ along direction ω_o, and $A_v(H_{\mathbf{x}}, \omega_o)$ is the visible area along this direction.

Then we can compute the integration over the visible part $A_v(H_{\mathbf{x}})$ with visibility function:

$$\int_{A_v(H_{\mathbf{x}})} dA_v(\omega_o) = \int_{A(H_{\mathbf{x}})} V(\mathbf{p}, \omega_o)(\mathbf{n} \cdot \omega_o) d\mathbf{p} \qquad (12)$$

Now with our triangle facet model at pixel $H(\mathbf{x})$, one facet f has the same normal direction $\mathbf{n}_f$. As a result the integration over $A(H_{\mathbf{x}})$ can be calculated within each facet area $A(f)$ and summed up:

$$\int_{A_v(H_{\mathbf{x}})} dA_v(\omega_o) = \sum_f \int_{A(f)} V(\mathbf{p}, \omega_o)(\mathbf{n} \cdot \omega_o) d\mathbf{p} \qquad (13)$$

The same scheme can be applied to the calculation of the visible projection area:

$$A(H_{\mathbf{x}}, \omega_o) = \sum_f \int_{A(f)} V(\mathbf{p}, \omega_o)(\mathbf{n}_f \cdot \omega_o) d\mathbf{p} \qquad (14)$$

Combining equation 10 and 13 into equation 11, we have:

$$\begin{aligned}
\bar{L}(H_{\mathbf{x}}, \omega_o) &= \frac{1}{A(H_{\mathbf{x}}, \omega_o)} \sum_f \int_{\Omega} \int_{A(f)} L_i(\omega_i) \rho(\mathbf{n}_f, \omega_i, \omega_o) \\
&\quad (\mathbf{n}_f \cdot \omega_i)(\mathbf{n}_f \cdot \omega_o) V(\mathbf{p}, \omega_i) V(\mathbf{p}, \omega_o) d\omega_i d\mathbf{p} \\
&= \int_{\Omega} L_i(\omega_i) \frac{\sum_f \gamma(f, \omega_i, \omega_o) \rho_f(\mathbf{n}_f, \omega_i, \omega_o)(\mathbf{n}_f \cdot \omega_o)}{A(H_{\mathbf{x}}, \omega_o)} (\mathbf{n}_f \cdot \omega_i) d\omega_i \\
&= \int_{\Omega} L_i(\omega_i) \bar{\rho}(H_{\mathbf{x}}, \omega_i, \omega_o)(\mathbf{n}_f \cdot \omega_i) d\omega_i
\end{aligned} \qquad (15)$$

Now we have the averaged BRDF for bi-scale material pixel $H_{\mathbf{x}}$

$$\bar{\rho}(H_{\mathbf{x}}, \omega_i, \omega_o) = \frac{\sum_f \gamma(f, \omega_i, \omega_o) \rho_f(\mathbf{n}_f, \omega_i, \omega_o)(\mathbf{n}_f \cdot \omega_o)}{A(H_{\mathbf{x}}, \omega_o)} \qquad (16)$$

where $\gamma(f, \omega_i, \omega_o)$ is the BFVF:

$$\gamma(f, \omega_i, \omega_o) = \int_{A(f)} V(\mathbf{p}, \omega_o) V(\mathbf{p}, \omega_i) d\mathbf{p} \qquad (17)$$